This article has been published in ISIJ International. The final publication is available at https://doi.org/10.2355/tetsutohagane.TETSU-2020-001

Evaluating the effect of the competition between NbC precipitation and grain size evolution on the hot ductility of Nb containing steels.

Kohei Furumai*, Xiang Wang*2, Hatem S. Zurob*2, and A.B.Phillion*2

*Steelmaking Research Dept., Steel Research Laboratory, JFE Steel Corporation, 1 Kokan-cho, Fukuyama, Hiroshima 721-8510

*2Department of Materials Science and Engineering, McMaster University, 1280 Main St West, Hamilton, ON, Canada, L8S 4L7

Keywords: continuous casting; Nb-containing steel; austenite grain growth; ferrite and austenite phases; precipitation; ductility; crack

Abstract

The hot ductility of steels containing 0-0.06wt.%Nb has been evaluated through γ grain growth experiments and hot stage tensile tests of the α+γ two phase region in order to clarify the roles of NbC precipitation and γ grain size evolution resulting from Nb-initiated solute drag on hot ductility in this important material property.

The experimental results show that (1) a decrease in γ grain size as a result of Nb-initiated solute drag improves hot ductility, (2) for a given γ grain size, hot ductility decreases with increasing Nb content because the corresponding increase in NbC precipitation fraction increases strength, and (3) the variation in ductility with Nb content is smaller when the γ grain size is smaller. These competing effects of γ grain size and NbC precipitation affect the strain incompatibility between the α and γ phases, leading to the onset of surface cracking during continuous casting when the incompatibility is high. The underlying mechanisms controlling ductility in Nb-containing steels are demonstrated using a model that partitions strain between the α and γ phases.

1. Introduction

Slab surface cracking is a particularly serious problem in the continuous casting of advanced high strength steels, deteriorating surface quality and decreasing productivity.[1] The cracks are believed to occur as a result of reduced ductility in the two phase (ferrite, α, and austenite, γ) region.[2-7] It has been reported that surface cracks are more likely to form in microalloyed steels, especially ones containing Nb, as compared to Nb-free steel. In Nb-free steels, the decrease in ductility (also known as embrittlement) is mainly

associated with the large γ grain size and the formation of film-like α along the γ grain boundaries.[8-11] In the case of Nb containing steel, there is evidence that Nb precipitation in the γ leads to additional loss of ductility and consequently enhances surface cracking.[2,4,10,12-15] However, it has been predicted that solute Nb can reduce embrittlement by reducing the rate of grain growth via the solute drag effect and leading to a finer γ grain size.[2,16-19] Thus, there is need to understand the effect of Nb on hot ductility and surface crack formation in terms of the competition between Nb precipitation and γ grain size in Nb containing steels.

In this study, the above concomitant phenomena affecting hot ductility are investigated for Nb contents from 0 to 0.06%. First, the evolution in γ grain size is quantified through grain growth experiments. Second, the hot ductility is quantified through hot tensile tests and correlated to γ grain size, Nb content, and NbC precipitation. Corresponding models are developed to investigate the underlying mechanisms controlling grain growth and hot ductility in Nb-containing steels.

2. Experimental Procedure

The chemical compositions of the steels used in this investigation are shown in Table 1, along with the corresponding equilibrium γ-to-α transformation temperature (Ae_3) calculated using the TCFE6 database[20] of THERMOCALC. The steels contain ~0.1%C and different Nb additions. Note that all compositions were analyzed by spark discharge atomic emission spectrometry and expressed in mass percent. To prepare the specimens for γ grain-growth experiments and hot tensile testing, all specimens were homogenized for 72 hours at 1100 ºC to break down the as-cast microstructure, and then austenitized twice for 60 s at 900 ºC followed by a water quench for grain refinement.[18] In order to estimate the initial γ grain size for subsequent grain-growth experiments, one of the specimens was austenitized a third time at 900 ºC, briefly, and then immediately quenched in water.

Grain Growth Experiments: γ grain-growth experiments were conducted at temperatures of 1100 ºC, 1200 ºC, 1300 ºC, and 1400 ºC, for holding times, t_h, of 300 to 4000 s. Following the isothermal treatment, the specimens were cooled at a rate of 0.07 ºC/s to 825 ºC, held at this temperature for 60 s, and then water quenched. The former γ grain boundaries were revealed using an aqueous solution of picric acid with sodium dodecylbenzene sulfonate and hydrochloric acid. [18,21] The microstructure was observed

by means of optical microscopy. The grain size was measured using the linear intercept method and the true three-dimensional grain diameter was estimated as being 1.61 times the linear intercept diameter.[22]

Hot Tensile Tests: The high temperature tensile tests were conducted using a Gleeble Thermo-mechanical system to evaluate the hot ductility in the $\alpha + \gamma$ phase. The sample geometry was cylindrical with a gauge diameter of 6 mm and a gauge length of 10 mm. The thermal cycle for the tensile tests involved heating to 1300 ºC and then holding for 50-2000 s (holding times, t_h',), in order to produce a range of γ grain-sizes. This was followed by cooling at 0.4, 1.0 or 50 ºC/s down to 825 ºC, holding for 60 s, and then deforming in tension until failure at a strain rate 2×10^{-3}/s. The thermomechanical processing schedule employed is summarized in Fig.1. A test temperature of 825˚C was chosen in order to understand the mechanisms of embrittlement during the initial stages of γ-to-α transformation, where the ductility of Nb-containing steels is low.[2,4] The reduction in area (RA) and the thickness of film-like α at the γ grain boundaries were measured from the fracture surfaces using optical microscopy.

The fracture morphologies of tensile test specimens were observed via scanning electron microscopy. Finally, a carbon extraction replica technique in conjunction with transmission electron microscopy (TEM) was used to quantify the size and number of Nb containing precipitations near the fracture surfaces.

3. Results

Example microstructures of two different steels, the Nb-free and the 0.06 %Nb after grain growth treatment for 300 and 4000s at 1200 ºC, are shown in Fig.2. As can be seen, the prior γ grains are clearly identified, allowing for accurate determination of the γ grain size. The results of grain size measurements at 1100, 1200, 1300, and 1400˚C are plotted in Fig. 3 as a function of t_h. Note that the standard deviation in the γ grain size was 11-23% of the average value. As can be seen, the grain size and grain growth rate increased with increasing test temperature and decreased with increasing Nb content.

The results of the hot ductility tests, specifically the RA are given in Fig. 4 as a function of Nb content and t_h' at a cooling rate of 1.0˚C/s. In the case of the same holding time, there is a clear decrease in RA with increasing Nb content, in agreement with previous report.[23] Fig. 5 shows the influence of the cooling rate on the measured ductility of holding time t_h' at 300s for all four steels. As can be seen, the RA decreased with

increasing cooling rate in all cases.

Fig. 6 shows the average thickness of the film-like α after deformation as a function of holding time t_h' for the tested steels and cooling rates. As can be seen, the average thickness of film-like α is independent of all three variables of holding time, cooling rate and composition. Since all the steels had a similar Ae_3 temperature (Table 1) and the same test temperature of 825 ˚C, the film-like α thickness would also be similar. Thus, although the film-like α, NbC precipitations, and γ grain size are all known to affect the hot ductility of Nb-containing steels, this study focused only on the latter two phenomena as the experiments did not allow for different α thicknesses. Examples of microstructures prior to and post tensile deformation are shown in Fig. 7 for Steel C (held at 1300˚C for 300s and then cooled at 1.0˚C/s to 825˚C). In the undeformed sample (a), no α is present, whereas in the deformed sample (b), a film-like α phase is present at the γ grain boundary along with an intergranular crack. It is considered that this phase formed immediately at the start of deformation because the average thickness of the film-like α was the same across all tests as shown in Fig. 6.

Fig. 8 shows the examples of fracture micrographs after tensile deformation at a holding time t_h' of 300s and a cooling rate of 1.0 ˚C/s for Steel A (a) and Steel C (b). Intergranular fractures were observed after deformation in the Nb-containing steels (Steel B, Steel C and Steel D) for the tested holding times and cooling rates. On the other hand, ductility dimple fractures were observed in the Nb-free steel (Steel A). From these results, it can be stated that intergranular crack took place in the Nb-containing steels (Steel B, Steel C and Steel D) of this study.

Fig. 9 shows an example TEM replica micrograph after 300s holding time at a cooling rate of 1.0 ˚C/s for steel C. As can be seen, the precipitations are oval shape, and easily identified from the background. EDS spectra identified these precipitations as NbC. Fig. 10 shows the relation between diameter and number density of the NbC precipitations found in Steel B, Steel C and Steel D with 300s holding time at a cooling rate of 1.0˚C/s. The total area of observation for each sample was 2.0 - $4.0 \times 10^{-11} m^2$. As can be seen, with increasing Nb content, the distribution shifts towards larger precipitations, i.e. towards the right.

4. Discussion

4.1. Quantification of the γ Grain Growth Kinetics

In order to evaluate the austenite grain mobility at different temperatures, a simple non-isothermal grain growth model was used,[24]

$$\frac{dr_c^2}{dt} = \frac{1}{2} M \gamma_{\mathrm{gb}}, \quad (1)$$

where r_c is the critical grain size as defined by Hillert[24] [m], t is time [s], M is a γ grain boundary mobility [m^4/s/J] and γ_{gb} is the grain boundary energy [J/m^2].[25] Eq. (1) is then integrated to obtain

$$r_c^2 = r_{c0}^2 + \frac{1}{2} M \gamma \Delta t. \quad (2)$$

where, r_{c0} is critical initial grain radius [m].

The critical grain size is related to the average grain size by the relation[24]

$$r_c = \frac{9}{8}\overline{r}, \; r_{c0} = \frac{9}{8}\overline{r}_0 \quad (3)$$

Eq. (3) is then substituted into Eq. (2) to give the expression

$$\overline{d}^2 = \overline{d}_0^{\,2} + 1.58 M \gamma_{gb} \Delta t, \quad (4)$$

where $\overline{d}$ is the average grain diameter [m] and $\overline{d}_0$ is the average initial grain diameter [m].

According to Turnbull's theory[26], the grain-boundary mobility can be expressed as

$$M_{pure}(T) = \frac{\delta V_m D_{GB}}{b^2 RT} = \frac{\delta V_m D_0 \exp\left(\frac{-Q}{RT}\right)}{b^2 RT}, \quad (5)$$

where M_{pure} is the intrinsic grain boundary mobility [m^4/s/J], δ is the grain boundary width [~1 nm][19], V_m is the molar volume [m^3/mol], b is the Burgers vector [m], R is the gas constant [J/K/mol], D_{GB} is the grain boundary diffusion coefficient [m^2/s], D_0 is the maximal diffusion coefficient at infinite temperature [m^2/s], Q is the diffusion activation energy [J/mol], and T is the absolutely temperature [K]. Using Eq. (4) and the grain growth kinetics given in Fig. 3, the grain boundary mobility, M was quantified at 1100, 1200, 1300, and 1400 ºC from the data for steel A. As this steel was Nb-free, the determined mobilities can be assumed to be the intrinsic values of γ grain-boundary mobility, M_{pure}, with reference to Nb. In order to quantify the temperature dependence of M_{pure}, the results were then fitted to a simplified form of Eq. (5), $M_{pure}(T) = \frac{A}{T} \cdot$

$\exp\left(-\frac{Q}{RT}\right)$, where A is a constant that includes the terms $\frac{\delta V_m D_0}{b^2 R}$. From the fitting exercise, $A = 0.26 \pm 0.06$ [m^{4}K/s/J]. The values of M_{pure} then range from 4.87×10^{-11} at 1100 ºC to 6.06×10^{-10} at 1400 ºC assuming $Q = 173156.6$ [J/mol] as reported by Zhou et al[18] for a similar C-Mn steel. The relative error is on the order of 10%.

The grain boundary mobility was then expressed as a function of the solute Nb content in order to quantify the effect of Nb on γ grain growth. According to Cahn's theory[27],

$$M' = \left(\frac{1}{M_{pure}} + \alpha_m C_{Nb}\right)^{-1} \qquad (6)$$

$$\text{with } \alpha_m = \frac{\delta N_v (k_b T)^2}{E_b D_x}\left(\sinh\left(\frac{E_b}{k_b T}\right) - \frac{E_b}{k_b T}\right), \qquad (7),$$

where M' is the grain boundary mobility in the presence of Nb [m^4/s/J], C_{Nb} is the atomic fraction of Nb in solution, N_v is the number of atoms per unit volume [m^{-3}], E_{b} is the binding energy of Nb to the grain-boundary [J/mol], D_{x} is the cross-boundary diffusion coefficient of Nb [m^2/s] and k_{b} is Boltzmann's constant [J/K]. The amount of solute Nb was estimated by using the TCFE6 database. The binding energy in Eq. (7) was taken to be 20kJ/mol.[28] The cross-boundary diffusion coefficient is much more difficult to estimate, and is discussed below.

Fig. 11 shows a comparison of the measured austenite grain size given in Fig. 3 at a holding time of 4000s (except for 1400 ºC, which used the 2000s data) and the modelled results as a function of Nb content. Following Rahman[18], the cross boundary diffusion coefficient was used as a fitting parameter assuming that the activation energy for cross-boundary diffusion is similar to that of Nb diffusion in the bulk γ phase[29]. Specifically, the pre-exponential constant for D_x was adjusted to fit the data. As can be seen in Fig. 11, Eqs. (4) through (8) provide a good description of the experimental grain growth data as a function of temperature and Nb content. Further, the results indicate the strong effect that Nb has on γ grain growth. Note that D_x was estimated to be

$$D_x = 0.000168 \cdot \exp\left(\frac{-2665}{RT}\right), \qquad (8)$$

which is twice the bulk value of the diffusivity of Nb reported by Kurokawa et al.[30]

4.2. Effect of γ Grain Size on Hot Ductility

Maehara et al[(2)] reported that the hot ductility, expressed as RA, is linearly proportional to the inverse of the γ grain size. This is confirmed in Fig. 12, which plots the measured RA as a function of $\overline{d_\gamma}^{-1}$ [mm-[1]] for each of the four steels with 50-2000s holding time at a cooling rate of 1.0 ºC /s. In all cases, the RA is seen to linearly decrease with decreasing inverse γ grain size. The relationship between RA and γ grain sizes varies depending on the Nb content. In order to quantify separately the effect of grain size and Nb content on RA, the slopes of each RA vs $\overline{d_\gamma}^{-1}$ curve from Fig. 12 are shown in Fig.13 as a function of Nb content. Although Fig. 12 showed that the hot ductility decreases with increasing Nb content at the same γ grain size, Fig. 13 shows that effect of γ grain size on RA increases with increasing Nb content. In other words, the drop in ductility with increasing Nb content is smaller when the γ grain size is smaller as shown in Fig. 12.

4.3. Effect of NbC precipitation on Hot Ductility

The relations between RA and average diameter of NbC precipitation, $\bar{d}_{ppt}^{NbC}$, phase fraction, f_{ppt}^{NbC}, and precipitation spacing, $\left(\rho_{ppt}^{NbC}\right)^{-1/3}$ where ρ_{ppt}^{NbC} is average number density of NbC precipitations [m^{-3}], for all four Nb compositions are shown in Figs. 14-16. The data were collected for the experiments performed at a holding time of 300s, and the results for each cooling rate are given as indicated by the numbers in parentheses. Note that in Fig. 15, the phase fraction was calculated via Eq. (9),

$$f_{ppt}^{NbC} = \frac{Total\ volum\ \ of\ NbC\ precipitates\ [m^3]}{Total\ area\ of\ observation\ [m^2] \times 2\bar{d}_{ppt}^{NbC}\ [m]} \cdot 100 \qquad (9)$$

where f_{ppt}^{NbC} is phase fraction of NbC precipitations [%]. This equation uses the NbC precipitation size distribution data to determine the total volume and assumes that the depth of the replica film is approximately twice the average precipitation diameter. Note also that none of $\bar{d}_{ppt}^{NbC}$, f_{ppt}^{NbC}, and $\left(\rho_{ppt}^{NbC}\right)^{-1/3}$ are independent since any one of these quantities could be expressed as a function of the other two.

Beginning with Fig. 14, it can be seen that in the case of the same composition, RA is reduced with a decrease in $\bar{d}_{ppt}^{NbC}$ resulting from an increase in the cooling rate. This

tendency matches the results reported by Crowther et al.[31] Further, as shown in Fig. 15, in the case of the same composition, RA is reduced with a decrease in f_{ppt}^{NbC} resulting from an increase in the cooling rate. This implies that a large precipitation volume fraction would improve the hot ductility, which does not agree with the bulk of the literature nor with the conclusions seen from Fig. 14.

The apparent contradiction in Figs. 14 and 15 can be resolved by considering that the effects of precipitations on strength requires one to consider both the precipitation fraction and the precipitation size. As such, neither figure offers a complete description of the effect of NbC precipitations on RA. A better understanding of the relevant mechanisms can be obtained by considering the strengthening contribution of precipitations. This could either be expressed in terms of $\sigma \sim \left(f_{ppt}^{NbC}\right)^{0.5} / \bar{d}_{ppt}^{NbC}$ in the case of particle bypass[32], or more simply as $\sigma \sim 1/L$ where L is the precipitation spacing. As can be seen in Fig. 16, RA decreases with decreasing $\left(\rho_{ppt}^{NbC}\right)^{-1/3}$. Since $L \propto \left(\rho_{ppt}^{NbC}\right)^{-1/3}$, the results in the figure demonstrate that the main strengthening mechanism in Nb-containing steels is precipitation strengthening[33]. Note that a secondary strengthening mechanism is the γ grain refinement, which is well-documented in Nb containing steels.

4.4. Ductility competition between ρ_{ppt}^{NbC} and grain size evolution

The competition between the ρ_{ppt}^{NbC}, and grain size evolution on the hot ductility of Nb-containing steels can be investigated using a strain partitioning model. The model is based on the assumption that a film-like α forms along the γ grain boundaries in the two phase (α+γ) region, and that cracking occurs along the γ grain boundaries. It has been reported that the partitioning of strain between the α and γ phases depends on the grain size and strain in γ and α,[4,34]

$$\varepsilon = \frac{d_\alpha}{\overline{d_\gamma}} \varepsilon_\alpha + \frac{\overline{d_\gamma} - d_\alpha}{\overline{d_\gamma}} \varepsilon_\gamma, \qquad (10)$$

where ε is the total strain, ε_α is the strain in the α layers , ε_γ is the strain in the γ grains, and d_α is the thickness of α layer along the γ boundary [mm].

The P ratio, $P = \frac{\varepsilon_\gamma}{\varepsilon_\alpha}$, provides a measure of strain incompatibility at the γ grain boundaries during deformation. By rearranging Eq. (10), the relationship between the global strain and the local incompatibility at the grain boundaries is obtained: [4]

$$\varepsilon = \varepsilon_\alpha \left\{ \frac{d_\alpha}{\overline{d_\gamma}} \left(1 - \frac{\varepsilon_\gamma}{\varepsilon_\alpha}\right) + \frac{\varepsilon_\gamma}{\varepsilon_\alpha} \right\} = \varepsilon_\alpha \left\{ \frac{d_\alpha}{\overline{d_\gamma}} (1 - P) + P \right\}. \quad (11)$$

In most steel alloys, the value of *P* is less than 1 because the flow stress of α is less than that of γ and thus strain concentrates in ferrite.[4] Under these conditions, failure should occur in the α layer and it can be assumed that the failure occurs when this strain reaches the critical α failure strain, $\varepsilon_{\alpha,f}$. The global strain when failure takes place, ε_f, is then obtained by substituting $\varepsilon_\alpha = \varepsilon_{\alpha,f}$ into Eq. (11),

$$\varepsilon_f = \varepsilon_{\alpha,f}\{D \cdot (1 - P) + P\}. \quad (12)$$

where the term $D = \frac{d_\alpha}{\overline{d_\gamma}}$ is introduced to represent the relative fractions of γ and α phases.

The effects of ρ_{ppt}^{NbC} and grain size can be examined by looking at the terms in Eq. (12), specifically the *D* and *P* ratios, both from mechanistic and mathematical perspectives. Mechanistically, the occurrence of Nb in solution within the γ grains decreases the γ grain size. As a result, the relative fraction of α increases, increasing the value of *D* and consequently increasing ε_f. Further, with increasing NbC precipitation, the strength of the γ phase is increased. This reduces the amount of deformation in this phase for a given applied load, and result in a decrease in *P*. Overall, the mechanistic effect of both ρ_{ppt}^{NbC} and γ grain size is to modify the partitioning of strain between α and γ. There is a secondary effect on the *P* ratio, that increasing the Nb content will also increase the underlying strength of the γ grains through solute strengthening and grain refinement (Hall Petch mechanism), and thus further decrease the value of *P*. Mathematically, it is shown through Eq.(12) that the equation's slope ($d_\alpha \cdot \varepsilon_{\alpha,f}(1 - P)$) of $\overline{d_\gamma}^{-1}$ increases with decreasing *P* and the equation's intercept ($\varepsilon_{\alpha,f} \cdot P$) decreases with decreasing *P*. Mechanistically, decreasing *P* corresponds to an increase in the Nb content. These relations are good agreement with the results shown in Fig. 12 and Fig. 13. Based on these results, it is important to optimize the NbC precipitation strengthening, the γ grain size and the thickness d_α covering the surface of γ grains to prevent surface crack formation during continuous casting.

5. Conclusions

The effect of Nb content on surface cracking during continuous casting has been examined through grain growth experiments and hot-stage tensile tests. There are two competing tendencies with increasing Nb content. The first is a decrease in γ grain size as a result of solute drag effect of Nb on grain boundary motion. In principle, the decrease in γ grain size reduces the strain incompatibility at γ/α grain boundaries and thus improves hot ductility and fewer surface cracks. On the other hand, as shown through this research, hot ductility decreases with increasing Nb content at the same γ grain size conditions. NbC precipitations due to an increase in Nb content increases the flow stress through precipitation strengthening, leading to a significant reduction in deformation within the γ grains as compared to the α grains. However, it is also confirmed that the effect of γ grain size on RA increases with increasing Nb content and the drop in ductility with Nb content is smaller when the γ grain size is smaller. Thus, the addition of Nb has a complex effect because it leads to γ grain refinement and NbC precipitations. Therefore, optimizing the NbC precipitation, the γ grain size and the thickness d_α covering the surface of γ grains, are important for preventing surface crack formation in Nb containing steel during continuous casting.

6. Acknowledgements

The authors acknowledge the assistance by the Natural Resources Canada Canmet Materials Laboratory in conducting the hot-stage tensile tests, and the Canadian Centre for Electron Microscopy (CCEM) at McMaster University for TEM measurement.

7. Tables

Table 1: Chemical composition of steels (mass %)

	[C]	[Nb]	[Mn]	[Si]	[P]	[S]	[Sol.Al]	[N]	Ae_3 [°C]
Steel A	0.098	-	0.97	0.30	0.012	0.0029	0.030	0.0026	856.4
Steel B	0.096	0.010	0.97	0.30	0.013	0.0028	0.029	0.0026	856.8
Steel C	0.098	0.030	0.96	0.30	0.012	0.0029	0.029	0.0026	857.7
Steel D	0.099	0.060	0.96	0.30	0.013	0.0030	0.030	0.0026	858.9

8. Figures

Figure 1: Thermal cycle experienced by samples undergoing hot stage tensile testing

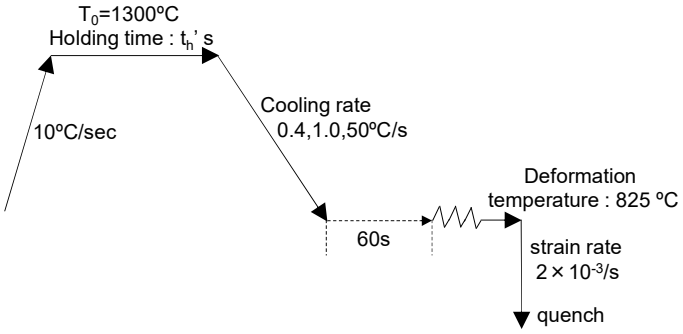

Figure 2: Micrographs showing the grain structure in the austenite grains after grain growth treatments of 300 s ((a), (c)) and 4000 s ((b), (d)) for Steel A and Steel D, respectively, at 1200°C

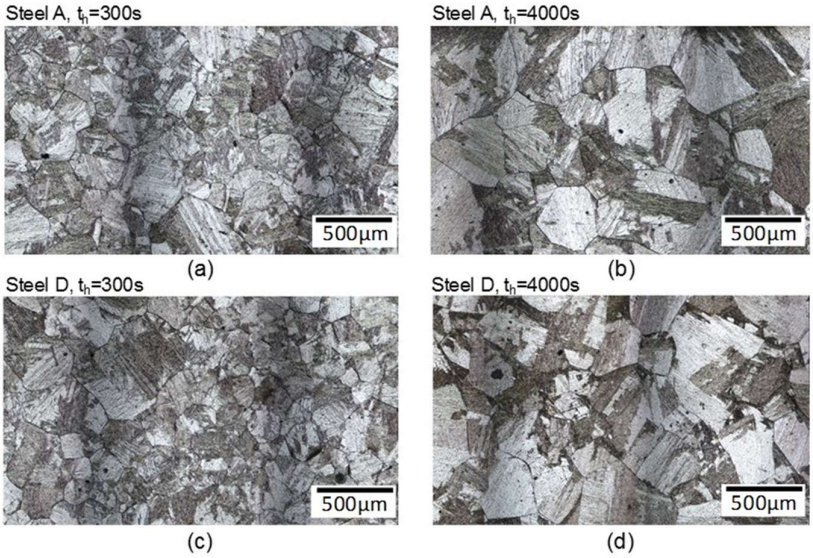

Figure 3: Measured austenite grain size as a function of holding time t_h at (a) 1100°C, (b) 1200°C, (c) 1300°C, and (d) 1400°C for all four steels

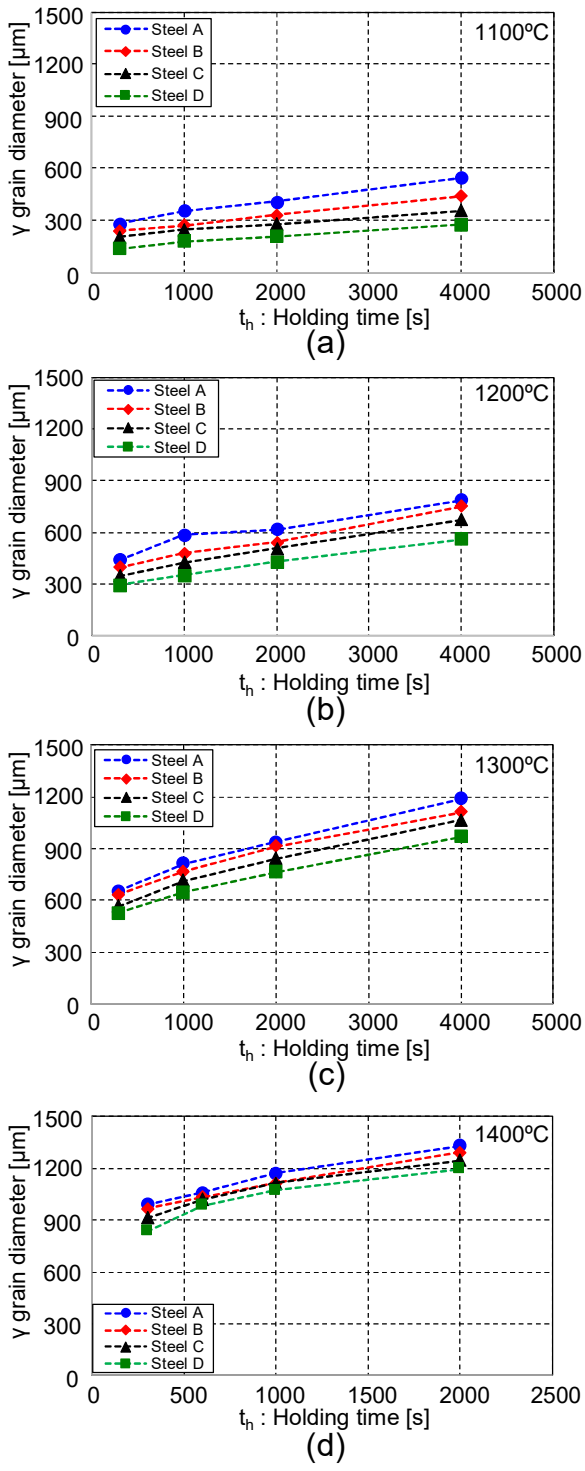

Figure 4: Influence of Nb content on the measured ductility at different holding times, t_h' of 50, 300, and 2000s for all four steels

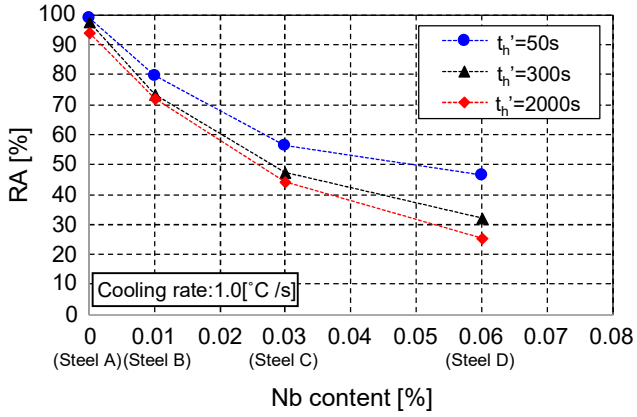

Figure 5: Influence of cooling rate on the measured ductility at a holding time t_h' of 300s for all four steels

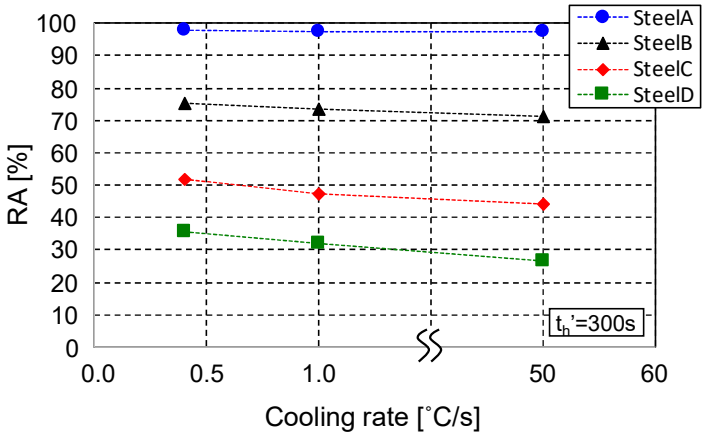

Figure 6: Average thickness of a film-like α for all four steels after deformation

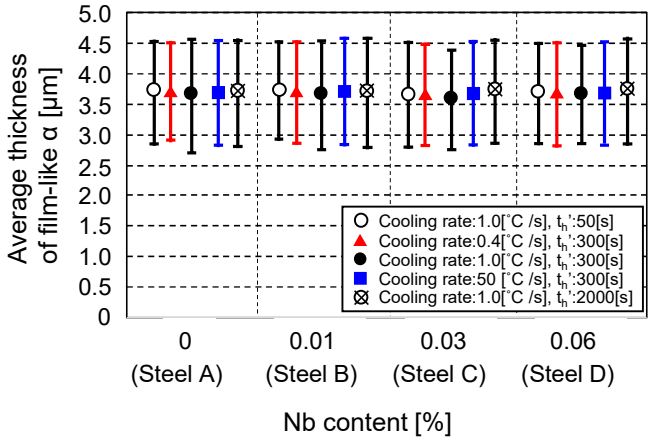

Figure 7: Microstructures (a) prior to and (b) post tensile deformation in Steel C

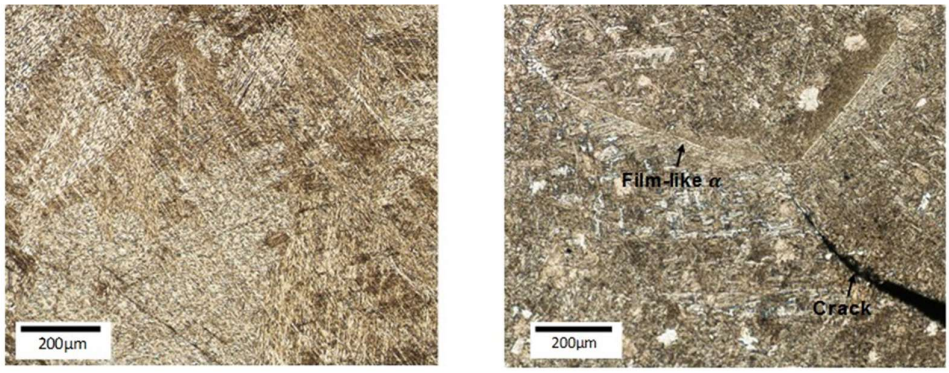

Figure 8: Fracture micrographs after tensile deformation at a holding time t_h' of 200s and a cooling rate of 1.0 [°C/s] for (a) Steel A and (b) Steel C

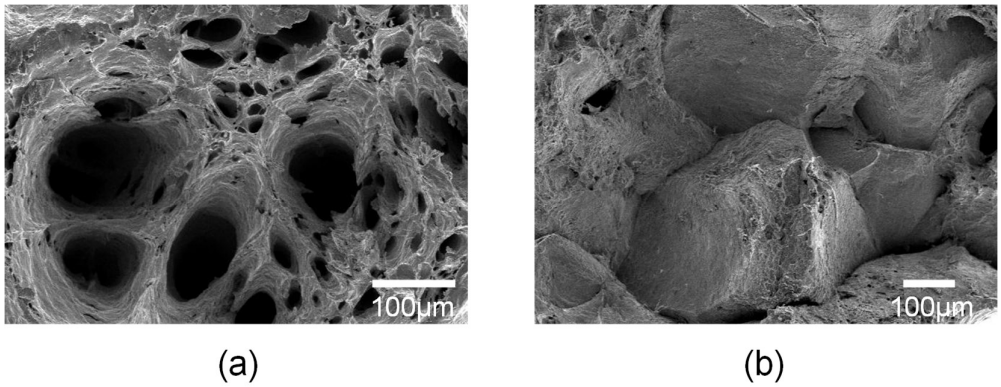

Figure 9: TEM replica micrograph in Steel C

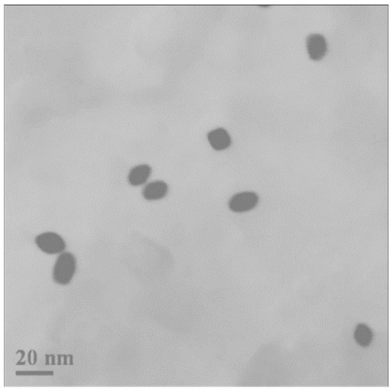

Figure 10: Number density of NbC precipitations in (a) Steel B, (b) Steel C, and (c) Steel D

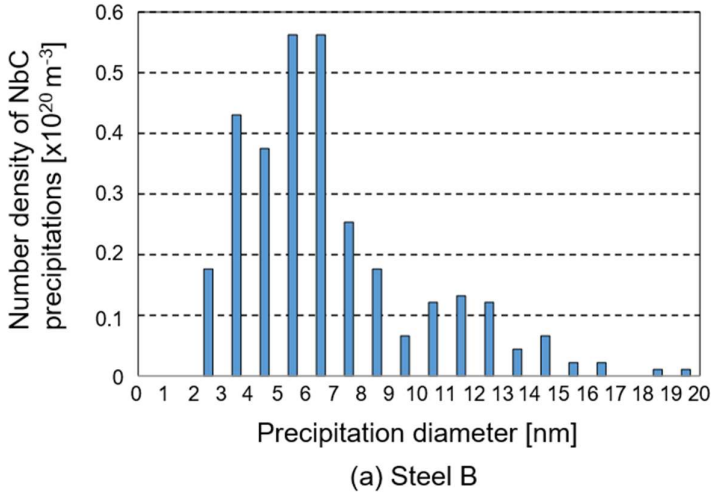

(a) Steel B

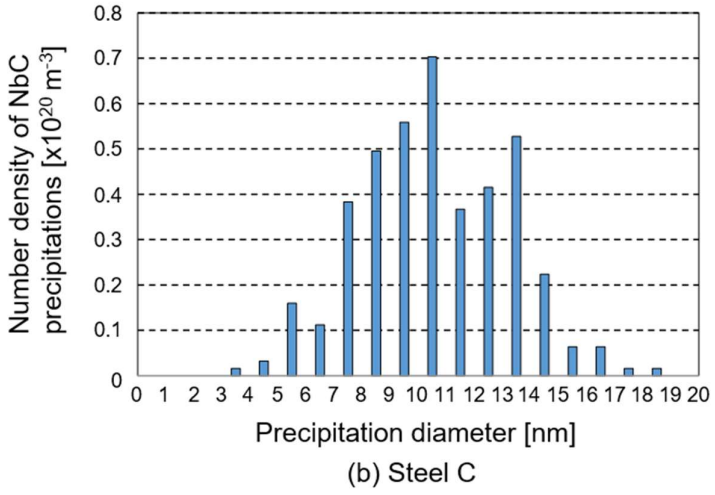

(b) Steel C

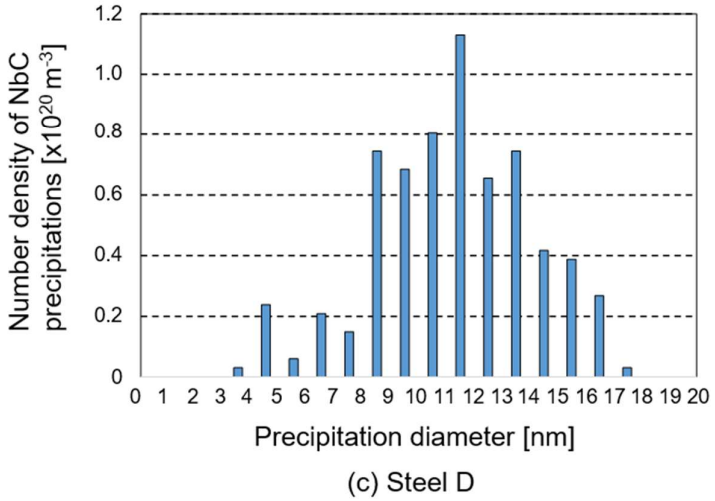

(c) Steel D

Figure 11: Comparison of the experimentally-measured austenite grain size (symbols) at a holding time of 4000 s (except for 1400°C, which used the 2000s data) and the modelled result (lines) as function of Nb content

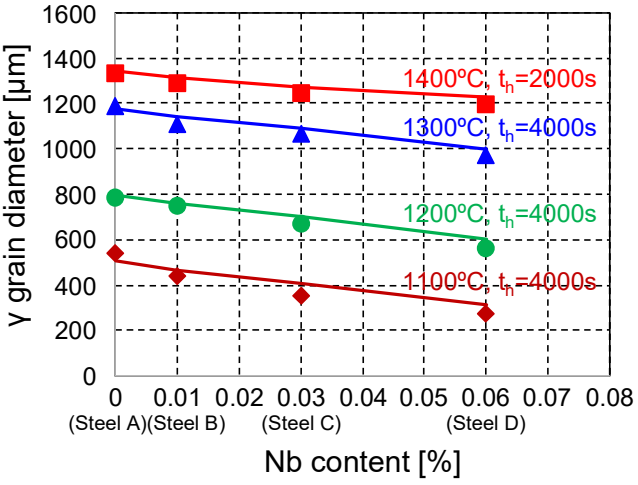

Figure 12: Measured ductility as a function of inverse austenite grain size, $\overline{d_\gamma}^{-1}$, for all four tested steels

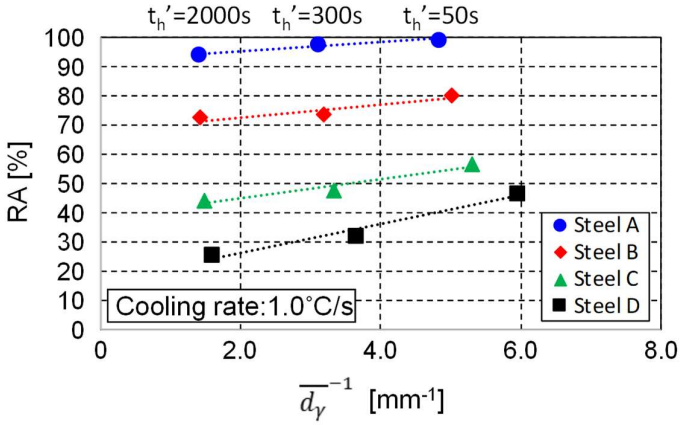

Figure 13: Influence of Nb content on the slope of the $\overline{d_\gamma}^{-1}$ vs. RA plot

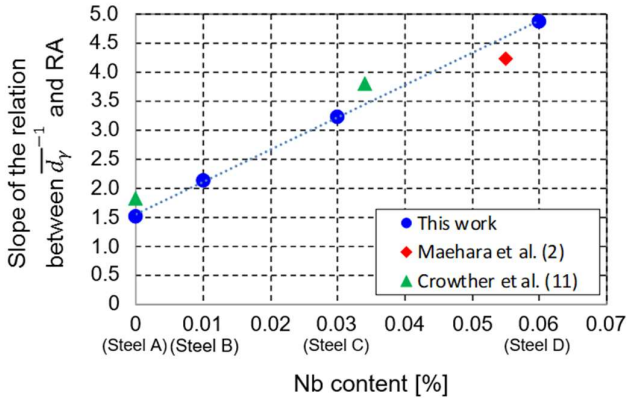

Figure 14: Relation between average diameter of NbC precipitation and RA

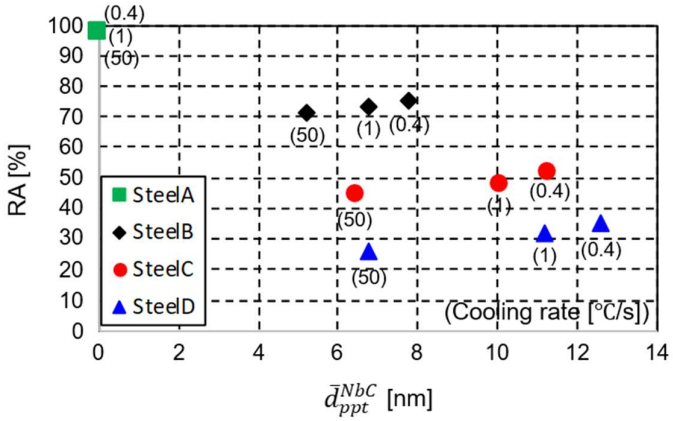

Figure 15: Influence of the phase fraction of NbC precipitations on RA

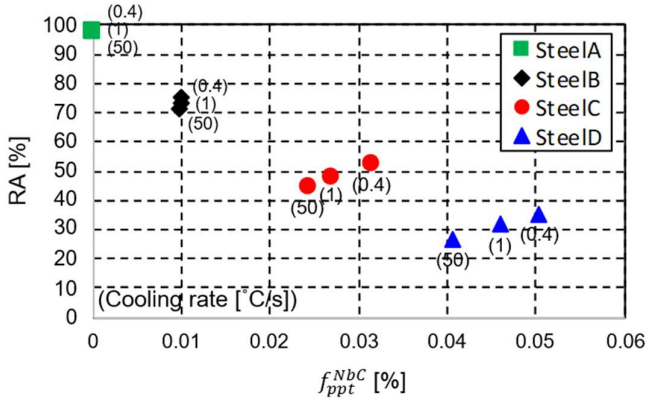

Figure 16: Relation between precipitation spacing ($L \propto \left(\rho_{ppt}^{NbC}\right)^{-\frac{1}{3}}$) and RA

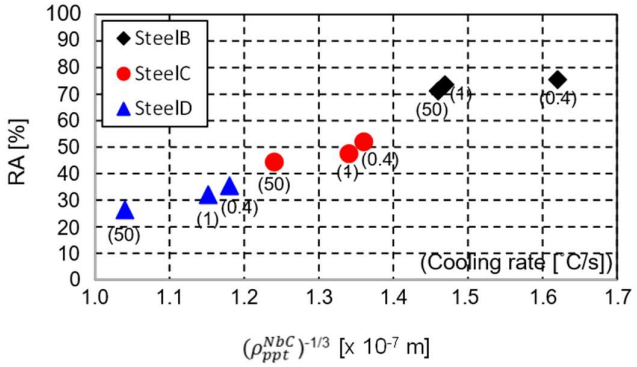

9. References

1) M.S. Kulkarni and A. Subash Babu: Journal of Materials Processing Technology, 166 (2005), 294.

2) Y. Maehara, K. Yasumoto, Y. Sugitani and K. Gumji: ISIJ Intl., 25 (1985), 1045.

3) H. G. Suzuki, S. Nishimura, J. Imamura and Y. Nakamura: Tetsu-to-Hagané, 67 (1981), 1180.

4) T. Maki, T. Nagamichi, N. Abe and I. Tamura: Tetsu-to-Hagané, 10 (1985), 1367.

5) F. J. Ma, G. H. Wen, P. Tang, X. Yu, J. Y. Li, G. D. Xu and F. Mei: Iron. & Steel., 37 (2010), 73.

6) K. M. Banks, A. S. Tuling and B. Mintz: Intl. J of Metall. Engg., 2 (2013), 188.

7) B. Mintz: ISIJ Intl., 39 (1999), 833.

8) Xiao Ping Li, Joong Kil Park, Joo Choi and Chang Hee Yim: Metals and Materials, 5 (1999), 25.

9) C. M. Chimani and K. Morwa: ISIJ Intl., 39 (1999), 1194.

10) B. Mintz, S. Yue and J. J. Jonas: Intl. Mater. Rev., 36 (1991), 187.

11) D. N. Crowther and B. Mintz: Mater. Sci. Technol., 2 (1986), 1099.

12) G Qian, G. Cheng and Z. Hou: ISIJ Intl., 54 (2014),1611.

13) K.R. Carpenter, R. Dippenaar and C.R. Killmore: Metall. Mater. Trans., 40A (2009), 573.

14) S. K. Kim, J. S. Kim and N. J. Kim: Metall. Mater. Trans., 33A (2002) 701.

15) K. Matsumoto, C. Ouchi and G. Tenmei: Tetsu-to-Hagané, 63 (1977), S722.

16) Y. Ogino, H. Tanida, M. Kitaura and A. Adachi: Tetsu-to-Hagané, 77 (1971), 533.

17) K. A. Alogab, D. K. Matlock, J. G. Speer and H. J. Kleebe: ISIJ Intl., 47 (2007), 307.

18) T. Zhou, R. J. O'malley and H. S. Zurob: Metall, Mater. Trans., 41A (2010), 2112.

19) M. K. Rehman and H. S. Zurob: Metall. Mater. Trans., 44A (2013), 1862.

20) Available from THERMO-CALC software, www.thermocalc.com.

21) G. F. V. Voort: Microsc. Microanal., 16 (2010), 774.

22) T. Gladman: Physical Metall. Microalloyed Steel, Inst. of Materials, London, (1997), 159.

23) K. Matsumoto and C. Ouchi: Tetsu-to-Hagané, 64 (1978), S286.

24) M. Hillert: Acta Metall., 13 (1965) 227.

25) H.S. Zurob, C.R. Hutchinson, Y. Brechet, and G. Purdy: Acta Mater., 50 (2002), 3075.

26) D. Turnbull: Trans. AIME, 1951, vol. 191, pp. 661–65.

27) J.W. Cahn: Acta Metall Mater., 24 (1976), 731.

28) H.S. Zurob, C.R. Hutchinson, Y. Brechet, and G. Purdy: Acta Mater., 50 (2002),

3075.
29) J. Geise and C. Herzig: Z. Metallk., 76 (1985), 622.
30) S. Kurokawa, J.E. Ruzzante, A.M. Hey and F. Dyment: Metals Science., 17 (1983), 433.
31) D.N. Crowther, Z. Mohamed and B. Mintz: ISIJ Intl., 27 (1987), 366.
32) V. Gerold, Dislocations in Solids, Amsterdam, 4 (1979), 219.
33) W.B. Morrison, J.H. Woodhead, J. Iron Steel. Inst., 201 (1963) 43.
34) M. Graf and E. Hornbogen: Acta Metall., 25 (1977), 883.